

A doubly stochastic matrices-based approach to optimal qubit routing

Nicola Mariella* Sergiy Zhuk*

November 15, 2022

Abstract

Swap mapping is a quantum compiler optimization that, by introducing SWAP gates, maps a logical quantum circuit to an equivalent physically implementable one. The physical implementability of a circuit is determined by the fulfillment of the hardware connectivity constraints. Therefore, the placement of the SWAP gates can be interpreted as a discrete optimization process. In this work, we employ a structure called doubly stochastic matrix, which is defined as a convex combination of permutation matrices. The intuition is that of making the decision process smooth. Doubly stochastic matrices are contained in the Birkhoff polytope, in which the vertices represent single permutation matrices. In essence, the algorithm uses smooth constrained optimization to slide along the edges of the polytope toward the potential solutions on the vertices. In the experiments, we show that the proposed algorithm, at the cost of additional computation time, can deliver significant depth reduction when compared to the state of the art algorithm SABRE.

1 Introduction

In the quantum computing field, the qubit routing procedure is a fundamental component of the quantum compiler. Its role is that of mapping logical qubits to physical ones while preserving the resulting unitary (up to a permutation) and fulfilling the connectivity constraints of the target hardware. The constraints consist of the set of pairs of physical qubits upon which a two-qubit gate can be applied. One of the methods for solving this problem is called swap mapping [10, 11].

The routing is obtained by introducing SWAP gates, which determine a permutation of the mapping between logical and physical qubits. The permutations are calculated so that the multi-qubit gates of the compiled circuit do not violate the connectivity restrictions of the hardware. In many architectures, the SWAP gate is constructed using three CNOTs, the latter, have usually a higher error rate [9] when compared to single-qubit gates. Moreover, adding gates to the circuit may enlarge the circuit depth, thus increasing decoherence-related issues. Consequently, the qubit routing is an optimization problem that not only is required to fulfill the hardware constraints, but also to minimize some function that depends on the number of added SWAPs and possibly the depth of the resulting circuit. In literature this problem is found under several designations, among others, we mention the qubit allocation, the layout synthesis and the qubit placement.

The computational complexity of the combinatorial problem behind the swap mapping has been proved in several forms. In [10] the mapping problem is formulated as a Hamiltonian cycle

*IBM Quantum, IBM Research Europe - Dublin

problem, resulting in being NP-complete. A reduction from the sub-graph isomorphism problem in [17] shows that the problem is NP-hard. This means that the design of practical algorithms should employ a heuristic component. Among the heuristics, remarkable is the SWAP-based BidiREctional (SABRE) algorithm [8]. At the time of writing, the latter is considered the state of the art and is currently the default swap mapping method for the Qiskit framework [1].

Despite the long-standing research on the topic, in [18] it was surveyed that, there is still a substantial optimality gap on the solutions produced by the most widespread tools for circuit synthesis.

In this work we present a swap mapping algorithm based on mathematical optimization and doubly stochastic matrices (DSM) [3]. Doubly stochastic matrices are convex combinations of permutations matrices. The intuition is that, since the qubit allocation makes use of swaps (permutations) we can model the decision process using a superposition of swap and identity matrices. Such superposition is then tuned by means of continuous parameters controlled by an optimizer. In addition, powerful algebraic properties of the resulting cost function allow the modeling of swap count and depth minimization. On the optimizer side, we propose a solver that scales linearly with the depth of the circuit, and our experiments show that for compiling quantum-volume circuits on 8 qubits our solver outperforms the state-of-the-art algorithm SABRE in terms of depth of the resulting circuit by 20 percentage points.

The paper is organized as follows. In Section 2 we introduce the basic definitions of the algebraic structures used throughout the formulation, Section 3.1 contains the construction of the fundamental part of the optimization problem — the hardware cost function. Sections 3.2, 3.3 and 3.4 expand on the optimization problem, its key features and the numerical method. In Section 4 we report the results from our experiments: numerical evaluation of the effect of algorithm’s hyper-parameters on compilation outcome, and comparisons against the state of the art algorithms. Finally the conclusions are elaborated in Section 5. All the proofs related to the main results can be found in the appendix.

2 Mathematical preliminaries

Notation. We introduce the basic notational conventions adopted throughout this work. We denote with \mathbb{I}_m the $m \times m$ identity matrix, also $\mathbf{1}_m$ denotes the vector of ones in the real vector space \mathbb{R}^m . Canonical basis vectors are identified with \mathbf{e}_i , also sometimes we highlight the dimension of the vector space by denoting with $\mathbf{e}_i^{(m)}$, the i -th (starting from zero) basis vector for \mathbb{R}^m . Given the relation with quantum computing we make use of the Dirac notation. In the context of this work, we interpret $|i\rangle_m$ as the i -th canonical basis vector for \mathbb{R}^m , that is $|i\rangle_m = \mathbf{e}_i^{(m)}$. Consequently, the outer product $|i\rangle_m \langle j|_m$ represents the rank-one matrix $\mathbf{e}_i^{(m)} \left(\mathbf{e}_j^{(m)} \right)^\top$. For a vector $\mathbf{v} \in \mathbb{R}^n$ and some integers i, j such that, $0 \leq i \leq j < n$ we denote with $\mathbf{v}[i \dots j]$ the sub-vector in \mathbb{R}^{j-i+1} obtained through the linear transformation

$$\mathbf{v}[i \dots j] = \sum_{k=0}^{m-1} |k\rangle_m \langle k+i|_n \mathbf{v}, \quad (1)$$

with $m = j - i + 1$. Given integers i, j such that $i \leq j$, we denote the set $[i, j] \cap \mathbb{Z}$ with $[i \dots j]$. The *Hadamard product* of $n \times m$ matrices A, B is denoted with $A \odot B$ and the resulting $n \times m$ matrix has entries $(A \odot B)_{i,j} = A_{i,j} B_{i,j}$, where $A_{i,j}$ denotes the matrix entry at the i -th row and j -th column.

Definition 1. We denote an $n \times n$ matrix A with non-negative entries, as doubly stochastic (DSM), when

$$AJ_n = J_n A = J_n, \quad (2a)$$

where $J_n = \mathbf{1}_n \mathbf{1}_n^\top$ is the $n \times n$ matrix of ones. In other words both rows and columns of A sum to 1 and $A_{i,j} \geq 0$. Moreover, the Birkhoff–von Neumann theorem [3] asserts that any doubly stochastic matrix can be decomposed as convex combination of permutation matrices, that is

$$A = \sum_{i=0}^{n!-1} \lambda_i P_i \quad (2b)$$

with $\lambda_i \geq 0$, $\sum_i \lambda_i = 1$ and $\{P_i\}$ the set of $n \times n$ permutation matrices.

We mention a well known result regarding the set of DSMs.

Lemma 2.1. The set of $n \times n$ doubly stochastic matrices form a monoid¹ under matrix multiplication.

Definition 2. Given any $n \times n$ matrix A , we define the row-major vectorization operator $\text{vec}_r : \mathcal{M}_{n,n}(K) \rightarrow K^n \otimes K^n$ with rule

$$\text{vec}_r(A) = \sum_{j=0}^{n-1} (A |j\rangle_n) \otimes |j\rangle_n = \sum_{i,j=0}^{n-1} A_{i,j} (|i\rangle_n \otimes |j\rangle_n), \quad (3a)$$

where $\mathcal{M}_{n,n}(K)$ is the set of $n \times n$ matrices over some field K . A special case is given by the identity matrix

$$\text{vec}_r(\mathbb{I}_n) = \sum_i |i\rangle_n \otimes |i\rangle_n, \quad (3b)$$

which can be interpreted as a Greenberger–Horne–Zeilinger state (GHZ) up to a scalar factor.

Lemma 2.2. Let A be any $n \times n$ matrix, then

$$\text{vec}_r(A) = (A \otimes \mathbb{I}_n) \text{vec}_r(\mathbb{I}_n) = (\mathbb{I}_n \otimes A^\top) \text{vec}_r(\mathbb{I}_n). \quad (4)$$

Proof in Appendix A.2. The next lemma presents some convenient identities that create a link between vectorization, tensor and Hadamard products and trace.

Lemma 2.3. Let A, B be any $n \times n$ matrices, then

$$\text{vec}_r(\mathbb{I}_n)^\top (A \otimes B) \text{vec}_r(\mathbb{I}_n) = \text{Tr}(AB^\top) \quad (5a)$$

$$= \mathbf{1}_n^\top (A \odot B) \mathbf{1}_n. \quad (5b)$$

Proof in Appendix A.2.

¹A monoid is defined as a set endowed with a binary associative operation and an identity element. In other words a monoid is a group without the inverse axiom. A counter-example to invertibility of DSMs is the following. Take X to be any permutation matrix that swaps two elements, then its eigenvalues are $\{-1, 1\}$, now $\frac{1}{2}(\mathbb{I}_n + X)$ is a DSM, but it has a zero eigenvalue, consequently it is singular.

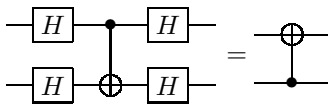


Figure 1: Reversal of the CNOT's control-target qubits.

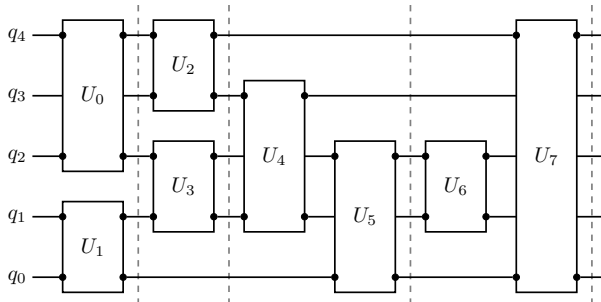


Figure 2: Example of commutative layering for a circuit of 2-qubit blocks. The blocks represent generic $U(4)$ unitaries where the dots identify the qubits upon which each unitary acts. The vertical dashed lines determine the layering, so for example take U_0 and U_1 from the first layer, then $(U_0 \otimes I^{\otimes 2})(I^{\otimes 2} \otimes U_1) = (I^{\otimes 2} \otimes U_1)(U_0 \otimes I^{\otimes 2})$, that is U_0, U_1 commute.

3 Main results

3.1 The hardware cost function

In this section we expand on the hardware cost function which, given a configuration of SWAP gates, vanishes when the composition of SWAPs and circuit layers fulfill the connectivity constraints.

Let \mathcal{M} represent the hardware graph, in which the vertices are interpreted as the physical qubits and the edges the connectivity between them. For simplicity we assume the connectivity to be undirected, also the graph \mathcal{M} is assumed connected² and nonempty. In the case of quantum technologies where the only 2-qubit gate is the CNOT gate, the reversal of the control-target of such gate (Figure 1) comes at no cost in terms of additional 2-qubit gates. Thus, the latter justifies the choice for the undirected graphs. We associate to graph \mathcal{M} the $m \times m$ adjacency matrix M . As consequence of the assumed structure of \mathcal{M} , we have that M is symmetric, that is $M = M^\top$. Let $J_m = \mathbf{1}_m \mathbf{1}_m^\top$ be the $m \times m$ matrix of ones, so denote $M_c = J_m - M$ the adjacency matrix of the *complement graph* to \mathcal{M} .

As outlined in [11], we decompose the circuit into layers of commuting two-qubits gates. An example of such circuit partitioning is presented in Figure 2. The same circuit is also presented in Figure 3 using a diagrammatic form that capture the essential information required for the swap mapping algorithm. Let $\mathcal{G}^{(t)}$ denote the graph corresponding to the layer at time step $t \in [0..T-1]$, and $G^{(t)}$ its adjacency matrix. The vertices of $\mathcal{G}^{(t)}$ correspond to the logical qubits, and the edges are the two qubit gates. Let $V_{\mathcal{G}^{(t)}}$ denote the set of vertices of the graph $\mathcal{G}^{(t)}$, then we impose $|V_{\mathcal{M}}| = |V_{\mathcal{G}^{(t)}}| = m$ and $V_{\mathcal{G}^{(t_1)}} = V_{\mathcal{G}^{(t_2)}}$ for all $t_1, t_2 \in [0..T-1]$.

Now, let P be an $m \times m$ permutation matrix, then we devise the following cost function for

²We should also assume that \mathcal{M} is not fully-connected otherwise the swap mapping would not be necessary.

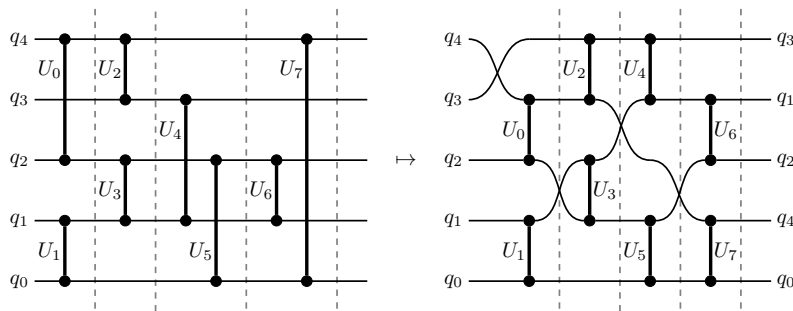


Figure 3: The braid diagram with gate arcs (left) corresponding to the circuit in Figure 2. In this example we assume the line connectivity, so on the right we propose a qubit allocation solution. Note on the right-hand side that the initial and final qubit layouts do not match. Here the braids on the right-hand side can be interpreted as the permutation of logical qubits (q_k) associated to physical ones (vertical positions).

layer t ,

$$\ell^{(t)}(P) = \mathbf{1}_m^\top \left[\left(PG^{(t)} P^\top \right) \odot M_c \right] \mathbf{1}_m \geq 0. \quad (6)$$

We observe that the global minima (also matching with zeros) of $\ell^{(t)}$ correspond to the permutations of the logical qubits such that the two-qubits gates overlap hardware arcs. In general the solution P to the problem of making $\ell^{(t)}(P)$ vanish is not unique, however later we will add a further restriction, that is the minimization of the number of SWAPs generating P .

We obtain an equivalent formulation for the cost function in (6). Using Lemmas 2.2 and 2.3 we have

$$\ell^{(t)}(P) = \text{Tr} \left(\left(PG^{(t)} P^\top \right) M_c^\top \right) \quad (7a)$$

$$= \text{Tr} \left(PG^{(t)} (M_c P)^\top \right) \quad (7b)$$

$$\stackrel{(5a)}{=} \text{vec}_r(\mathbb{I}_m)^\top \left(PG^{(t)} \right) \otimes (M_c P) \text{vec}_r(\mathbb{I}_m) \quad (7c)$$

$$= \text{vec}_r(\mathbb{I}_m)^\top (\mathbb{I}_m \otimes M_c) (P \otimes P) \left(G^{(t)} \otimes \mathbb{I}_m \right) \text{vec}_r(\mathbb{I}_m) \quad (7d)$$

$$\stackrel{(4)}{=} \text{vec}_r(M_c)^\top (P \otimes P) \text{vec}_r(G^{(t)}), \quad (7e)$$

The new form in (7e) is convenient for the theory that follows, the key fact is that the cost function is now linear with respect to $P \otimes P$. The intent is that of obtaining a cost value as a superposition of cost values (non-negative) for individual solutions. Specifically, each solution is determined by a permutation matrix P_i , then given a set of candidate solutions $\{P_i\}$ we obtain the convex combination

$$\sum_i \lambda_i \ell^{(t)}(P_i) = \sum_i \lambda_i \text{vec}_r(M_c)^\top (P_i \otimes P_i) \text{vec}_r(G^{(t)}) \quad (8a)$$

$$= \text{vec}_r(M_c)^\top \left(\sum_i \lambda_i (P_i \otimes P_i) \right) \text{vec}_r(G^{(t)}), \quad (8b)$$

with $\boldsymbol{\lambda} \in \Delta_S$ where Δ_S is the *unit simplex* in S dimensions [2]. In (8b) we have the first appearance of an interesting structure, whose characterization is given by the following lemma.

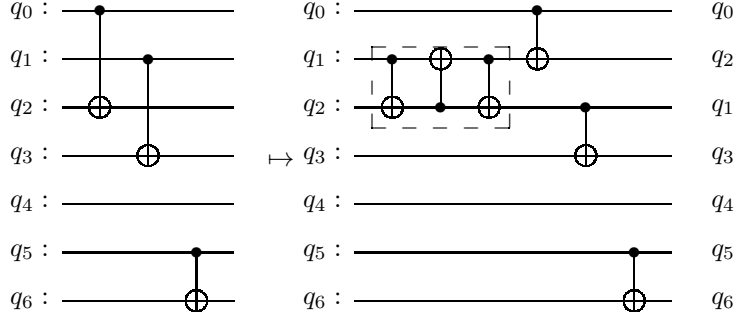


Figure 4: On the left-hand side, a circuit layer corresponding to the adjacency matrix $G^{(t)}$ considered in Figure 5. Note that the CNOTs commute. On the right-hand side, the circuit after the application of the swap (highlighted).

Lemma 3.1. *Let $Q = \sum_i \lambda_i P_i$ be a doubly stochastic matrix, where P_i are $m \times m$ permutation matrices. Then*

$$K = \sum_i \lambda_i P_i \otimes P_i \quad (9)$$

is doubly stochastic.

Proof in Appendix A.2.

The function $\ell^{(t)}(P)$ is the key component of what will be defined later as the *hardware cost function*. In Figure 5 we provide a visual example of the cost function machinery, also Figure 4 presents the circuit related to the example matrices.

Remark 3.1. We highlight again the linearity of the optimization problem determined by (8a). Take for simplicity the problem of minimizing the hardware cost function for the layer t . Consider m qubits and fix the set of permutation matrices $\{P_i\}$ corresponding to the representations of the elements of the symmetric group \mathcal{S}_m . Then the problem takes the form

$$\min_{\lambda \in \mathbb{R}^{m!}} \sum_{i=0}^{m!-1} \lambda_i \ell^{(t)}(P_i), \quad (10a)$$

$$\text{s.t. } \lambda_i \geq 0 \quad \forall i, \quad (10b)$$

$$\sum_i \lambda_i = 1. \quad (10c)$$

The latter is clearly a linear problem over a convex set, however the difficulty arises from the cardinality $m!$ of the set of permutations. We avoid this difficulty by introducing a construction that produces a subgroup of permutations controlled by a polynomial number of parameters (w.r.t. m).

△

The machinery for the swapping requires consistency between layers, that is, we have to assure the connectivity of logical qubits as we pass from one layer to the next. Let $P^{(t)}$ be the permutation applied before the layer at time step t , for all $t \in [0..T-1]$. We define the finite sequence $(C^{(t)})_{t \in [0..T-1]}$ of permutations composed up to time t as

$$C^{(0)} = P^{(0)}, \quad (11a)$$

$$C^{(t)} = P^{(t)} C^{(t-1)}, \quad 1 \leq t \leq T-1, \quad (11b)$$

$$\begin{aligned}
M &= \begin{pmatrix} \bullet & \bullet & \cdot & \cdot & \cdot & \cdot & \cdot & \cdot \\ \bullet & \bullet & \bullet & \cdot & \cdot & \cdot & \cdot & \cdot \\ \cdot & \bullet & \bullet & \bullet & \cdot & \cdot & \cdot & \cdot \\ \cdot & \cdot & \bullet & \bullet & \bullet & \cdot & \cdot & \cdot \\ \cdot & \cdot & \cdot & \bullet & \bullet & \bullet & \cdot & \cdot \\ \cdot & \cdot & \cdot & \cdot & \bullet & \bullet & \bullet & \cdot \\ \cdot & \cdot & \cdot & \cdot & \cdot & \bullet & \bullet & \bullet \end{pmatrix}, & G^{(t)} &= \begin{pmatrix} \cdot & \cdot & \bullet & \cdot & \cdot & \cdot & \cdot & \cdot \\ \cdot & \cdot & \cdot & \bullet & \cdot & \cdot & \cdot & \cdot \\ \bullet & \cdot & \cdot & \cdot & \cdot & \cdot & \cdot & \cdot \\ \cdot & \bullet & \cdot & \cdot & \cdot & \cdot & \cdot & \cdot \\ \cdot & \cdot & \cdot & \cdot & \cdot & \cdot & \cdot & \cdot \\ \cdot & \cdot & \cdot & \cdot & \cdot & \cdot & \cdot & \bullet \\ \cdot & \cdot & \cdot & \cdot & \cdot & \cdot & \cdot & \bullet \end{pmatrix}, \\
P &= \begin{pmatrix} \bullet & \cdot & \cdot & \cdot & \cdot & \cdot & \cdot & \cdot \\ \cdot & \cdot & \bullet & \cdot & \cdot & \cdot & \cdot & \cdot \\ \cdot & \bullet & \cdot & \cdot & \cdot & \cdot & \cdot & \cdot \\ \cdot & \cdot & \cdot & \bullet & \cdot & \cdot & \cdot & \cdot \\ \cdot & \cdot & \cdot & \cdot & \bullet & \cdot & \cdot & \cdot \\ \cdot & \cdot & \cdot & \cdot & \cdot & \bullet & \cdot & \cdot \\ \cdot & \cdot & \cdot & \cdot & \cdot & \cdot & \bullet & \cdot \\ \cdot & \cdot & \cdot & \cdot & \cdot & \cdot & \cdot & \bullet \end{pmatrix}, & PG^{(t)}P^\top &= \begin{pmatrix} \cdot & \bullet & \cdot & \cdot & \cdot & \cdot & \cdot & \cdot \\ \bullet & \cdot & \cdot & \cdot & \cdot & \cdot & \cdot & \cdot \\ \cdot & \cdot & \bullet & \cdot & \cdot & \cdot & \cdot & \cdot \\ \cdot & \cdot & \cdot & \bullet & \cdot & \cdot & \cdot & \cdot \\ \cdot & \cdot & \cdot & \cdot & \bullet & \cdot & \cdot & \cdot \\ \cdot & \cdot & \cdot & \cdot & \cdot & \bullet & \cdot & \cdot \\ \cdot & \cdot & \cdot & \cdot & \cdot & \cdot & \bullet & \cdot \\ \cdot & \cdot & \cdot & \cdot & \cdot & \cdot & \cdot & \bullet \end{pmatrix}.
\end{aligned}$$

Figure 5: In this example we illustrate the matrices involved in (6). We define graphically with \cdot, \bullet the values 0, 1 respectively. In the circuit adjacency matrix $G^{(t)}$ (corresponding to left part of Figure 4) we see that some of the non-zero entries do not overlap with the hardware topology M . However, after applying the permutation P we see that the total overlap is established in $PG^{(t)}P^\top$, hence $\ell^{(t)}(P)$ vanishes.

expanded, the sequence takes the following form

$$\begin{aligned}
C^{(0)} &= P^{(0)}, \\
C^{(1)} &= P^{(1)}P^{(0)}, \\
&\vdots \\
C^{(T-1)} &= P^{(T-1)} \dots P^{(1)}P^{(0)}.
\end{aligned}$$

Given a sequence of permutations $(P^{(t)})_{t \in [0..T-1]}$ we obtain the *hardware cost function* for the overall circuit, so

$$\mathcal{L} \left((P^{(t)})_t \right) = \sum_{t=0}^{T-1} \ell^{(t)} \left(C^{(t)} \right), \tag{12}$$

Note that the sequence $(C^{(t)})_t$ depends on $(P^{(t)})_t$.

again it can be shown that the global minima (zeros) correspond to the set of permutations that implements the circuit on allowable hardware arcs (the edges of graph \mathcal{M}). In relation to Figure 3, the permutations $P^{(t)}$ correspond to the braids, and the graphs $\mathcal{G}^{(t)}$ match the layers with the gate arcs implementing the edges.

The limited connectivity of the hardware structure³ implies that the permutations $P^{(t)}$ must be generated by the swaps corresponding to the directly connected vertices of graph \mathcal{M} . However, before expanding the aforementioned restriction we first proceed with the definition of SWAP. Let m be the number of qubits of the circuit and assume $m \geq 2$. We define the swap operator w.r.t. distinct vertices $i, j \in [0..m-1]$, as

$$\text{SWAP}_m(i, j) := \mathbb{I}_m - |i\rangle_m \langle i|_m - |j\rangle_m \langle j|_m + |i\rangle_m \langle j|_m + |j\rangle_m \langle i|_m, \tag{13}$$

³The hardware graph \mathcal{M} is assumed to be not fully-connected.

equivalently the operator is determined by its action on the vectors $|k\rangle_m$ with $k \in [0..m-1]$,

$$\text{SWAP}_m(i, j) |k\rangle_m = \begin{cases} |j\rangle_m, & k = i, \\ |i\rangle_m, & k = j, \\ |k\rangle_m, & \text{otherwise.} \end{cases}$$

Remark 3.2. The SWAP_m defined in (13) should be considered as the classical counterpart of the swap operator SWAP_m^Q in the context of quantum circuits. The $\text{SWAP}_m(i, j)$ operator acts on a space having dimension m , also the result of its action is the swap of the the basis vectors $|i\rangle_m$ and $|j\rangle_m$. The $\text{SWAP}_m^Q(i, j)$ instead, acts on a space of dimension 2^m and its action swaps 2^{m-1} basis vectors. The latter is represented diagrammatically using the symbol $\overleftrightarrow{\text{I}}$, however in the context of this work, the same symbol is used to indicate both operators interchangeably. \triangle

We obtain the set of generators for the permutations implementing the swap mapping, so

$$\mathcal{P}_{\mathcal{M}} = \{\text{SWAP}_m(i, j) | M_{i,j} = 1, i < j\}, \quad (14)$$

where M is the adjacency matrix for the hardware couplings. In other words, each permutation $P^{(t)}$ for layer t , is constructed by composing a subset of elements of $\mathcal{P}_{\mathcal{M}}$. Later we will introduce an objective that aims at minimizing the number of elements of such construction.

We extend again the approach by introducing a sort of 'smooth swap', that is a swap operator in superposition with the identity. We define the *smooth swap* operator $\text{SSWAP}_m(i, j, \theta)$ as one of the following equivalent forms

$$\text{SSWAP}_m(i, j, \theta) := \cos^2(\theta)\mathbb{I}_m + \sin^2(\theta)\text{SWAP}_m(i, j) \quad (15a)$$

$$= \mathbb{I}_m + \sin^2(\theta) (\text{SWAP}_m(i, j) - \mathbb{I}_m) \quad (15b)$$

$$= \mathbb{I}_m + \sin^2(\theta) (|i\rangle_m \langle j|_m + |j\rangle_m \langle i|_m - |i\rangle_m \langle i|_m - |j\rangle_m \langle j|_m), \quad (15c)$$

which can be shown to be *convex combinations* of the identity matrix and the swap acting on vertices i, j . It follows from the Birkhoff–von Neumann theorem that $\text{SSWAP}_m(i, j, \theta)$ is a *doubly stochastic matrix* [7]. The specific structure of the matrix $\text{SSWAP}_m(i, j, \theta)$ is also known as an *elementary doubly stochastic matrix* [3]. By Lemma 2.1, the set of DSM of the same size is closed under matrix multiplication, so by composing multiple SSWAP operators we obtain another matrix of the same class. Notably, in our case, when the θ s are integer multiples of $\frac{\pi}{2}$ we obtain a vertex of the *Birkhoff polytope*, that is a permutation matrix. This means that we can substitute the component $P \otimes P$ in (7e) with a composition (depending on some hyper-parameters) of operators of the form,

$$\text{PSSWAP}_m(i, j, \theta) := \cos^2(\theta)\mathbb{I}_m^{\otimes 2} + \sin^2(\theta)\text{SWAP}_m(i, j)^{\otimes 2} \quad (16a)$$

$$= \mathbb{I}_m^{\otimes 2} + \sin^2(\theta) (\text{SWAP}_m(i, j)^{\otimes 2} - \mathbb{I}_m^{\otimes 2}) \quad (16b)$$

$$= \frac{1}{2} (\mathbb{I}_m^{\otimes 2} + \text{SWAP}_m(i, j)^{\otimes 2}) + \frac{\cos(2\theta)}{2} (\mathbb{I}_m^{\otimes 2} - \text{SWAP}_m(i, j)^{\otimes 2}). \quad (16c)$$

Note that here we extended the concept of SSWAP to that of PSSWAP , where the prefix P stands for 'parallelized' which resembles the effect of the tensor power. In the next section we continue with the substitution of the PSSWAP in the cost function (12), resulting in the weighted sum of costs corresponding to the superposition of solutions determined by the parameters θ s.

Remark 3.3. In relation to the definition of PSSWAP , we highlight that in general

$$\text{PSSWAP}(i, j, \theta) \neq \text{SSWAP}_m(i, j, \theta)^{\otimes 2}. \quad (17)$$

\triangle

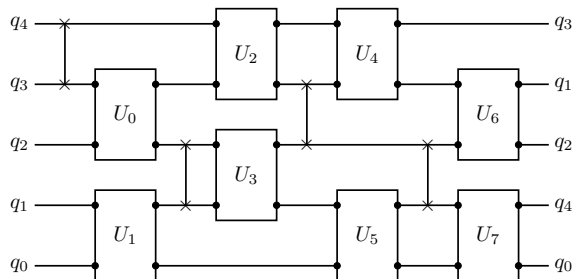


Figure 6: The final circuit corresponding to the input circuit in Figure 2.

3.2 The optimization problem: formulation

We start by defining the constructor generating the permutations $P^{(t)}$ at each time step t . We recall that we denote by T the number of layers of the input circuit, so the layer index t belongs to $[0..T-1]$. Also each layer determines S continuous parameters, so overall we have $S \times T$ parameters, which will be denoted by $\theta \in \mathbb{R}^{ST}$.

The constructor configuration (hyper-parameters) is a pair (p_1, p_2) of functions $p_1, p_2 : [0..S-1] \rightarrow V_{\mathcal{M}}$ mapping a sequence index s to a physical qubit⁴. Moreover, in the scope of this section we consider the functions (p_1, p_2) as arbitrary, however Section 3.3 will develop a specific structure for them. At each time step t the hyper-parameters determine a sequence of S swaps $\text{SSWAP}_m(p_1(s), p_2(s), \theta_s^{(t)})$ for $s \in [0..S-1]$. So, given a vector of continuous parameters $\theta = \left(\theta_s^{(t)} \right)_{t,s} \in \mathbb{R}^{ST}$, the hardware cost function assumes the form

$$\mathcal{L}(\theta) = \sum_{t=0}^{T-1} \mathcal{L}_t(\theta), \quad (18)$$

with

$$\mathcal{L}_t(\theta) = \beta(t) \text{vec}_r(M_c)^\top K^{(t)} \text{vec}_r(G^{(t)}), \quad (19a)$$

and

$$P^{(t)} = \text{PSSWAP}_m(p_1(0), p_2(0), \theta_0^{(t)}) \cdots \text{PSSWAP}_m(p_1(S-1), p_2(S-1), \theta_{S-1}^{(t)}), \quad (19b)$$

$$K^{(0)} = P^{(0)}, \quad (19c)$$

$$K^{(t)} = P^{(t)} K^{(t-1)}, \quad 1 \leq t \leq T-1. \quad (19d)$$

In (18), each term is scaled by the function $\beta : \mathbb{R} \rightarrow \mathbb{R}$ which is assumed decreasing and positive valued. The function β , is one of the key components of the heuristic solver — the *adaptive feasibility*, which is introduced in Section 3.4. Note that each continuous parameter $\theta_s^{(t)}$ appears as PSSWAP argument, one time for all terms in (18) such that $t \geq t_1$. Also $\mathcal{L}(\theta) \geq 0$ for all θ .

We obtain the ideal form for the optimization problem, that is

$$\begin{aligned} \min_{\theta \in \mathbb{R}^{ST}} \quad & \text{card}(\theta), \\ \text{s.t.} \quad & \mathcal{L}(\theta) = 0, \end{aligned} \quad (20)$$

⁴We also require that $i = p_1(s) \neq p_2(s) = j$ for all s , so we always have distinct targets $\{i, j\}$ for the swap.

where $\mathbf{card}(\boldsymbol{\theta})$ is the cardinality⁵ of the vector $\boldsymbol{\theta}$. The structure of the problem is justified by the fact that for $\theta_s^{(t)} = 0$, the corresponding PSSWAP is the identity permutation. The next proposition shows that an optimization problem with cardinality as objective and whose constraint matches a certain structure, can be solved by an equivalent differentiable problem.

Proposition 3.2. *Given the structure of the hardware cost function \mathcal{L} , the following optimization problems are equivalent*

$$\left\{ \begin{array}{l} \min_{\boldsymbol{\theta} \in \mathbb{R}^{ST}} \|\boldsymbol{\theta}\|_2^2, \\ \text{s.t.} \quad \mathcal{L}(\boldsymbol{\theta}) = 0, \end{array} \right. \cong \left\{ \begin{array}{l} \min_{\boldsymbol{\theta} \in \mathbb{R}^{ST}} \mathbf{card}(\boldsymbol{\theta}), \\ \text{s.t.} \quad \mathcal{L}(\boldsymbol{\theta}) = 0. \end{array} \right. \quad (21)$$

Proof in Appendix A.2. This proposition demonstrates that the problem in (20) can be solved by considering the squared l_2 -norm of $\boldsymbol{\theta}$ instead of its cardinality.

Let us study the characterization of the stationary points of the hardware cost function \mathcal{L} . The next proposition shows that vectors $\boldsymbol{\theta} \in \mathbb{R}^{ST}$ such that the individual elements are integer multiples of $\frac{\pi}{2}$, are a sufficient condition for the stationary points of the hardware cost function.

Proposition 3.3. *Consider the hardware cost function (18) and the element $\theta_s^{(t)}$ with index (s, t) belonging to the vector $\boldsymbol{\theta} \in \mathbb{R}^{ST}$. Let $\Omega = \{k\frac{\pi}{2} | k \in \mathbb{Z}\}$ be the set of integer multiples of $\pi/2$. Then*

$$1. \quad \boldsymbol{\theta}^\top \mathbf{e}_s^{(t)} \in \Omega \implies \frac{\partial \mathcal{L}(\boldsymbol{\theta})}{\partial \theta_s^{(t)}} = 0.$$

If $\frac{\partial \mathcal{L}(\bar{\boldsymbol{\theta}})}{\partial \theta_s^{(t)}} = 0$, for some $\bar{\boldsymbol{\theta}} \in \mathbb{R}^{ST}$, then, either

$$2. \quad \bar{\boldsymbol{\theta}}^\top \mathbf{e}_s^{(t)} \in \Omega,$$

$$3. \quad \text{or } \bar{\boldsymbol{\theta}}^\top \mathbf{e}_s^{(t)} \notin \Omega \text{ and } \frac{\partial \mathcal{L}(\hat{\boldsymbol{\theta}})}{\partial \theta_s^{(t)}} = 0 \text{ for } \hat{\boldsymbol{\theta}} \in \{\bar{\boldsymbol{\theta}} + r\mathbf{e}_s^{(t)} | r \in \mathbb{R}\}.$$

Proof in Appendix A.2.

Remark 3.4. Note that Case 3 of Proposition 3.3 proposition suggests that the constraint is locally “flat” in the direction \mathbf{e}_s which means that multiple solutions are possible, but this ambiguity is resolved by 2-norm minimization which simply picks 0 in this case. Let us further illustrate Case 3: given circuits C_1 and C_2 , we define the equivalence relation $C_1 \sim C_2$ whenever the circuits implement the same unitary up to a permutation. Now, assume the line connectivity and consider the swap mapping process that follows.

$$\begin{array}{c} q_0 : \text{---} \bullet \text{---} \\ q_1 : \text{---} \text{---} \\ q_2 : \text{---} \oplus \text{---} \end{array} \xrightarrow{\text{SWAP}} \begin{array}{c} q_0 : \text{---} \times \text{---} \\ \quad \quad \quad \theta_0 \\ q_1 : \text{---} \times \text{---} \bullet \text{---} \\ q_2 : \text{---} \oplus \text{---} \end{array} \quad q_1 \sim \begin{array}{c} q_0 : \text{---} \times \text{---} \\ \quad \quad \quad \theta_0 \\ q_1 : \text{---} \times \text{---} \oplus \text{---} \\ \quad \quad \quad \theta_1 \\ q_2 : \text{---} \times \text{---} \bullet \text{---} \end{array} \quad q_0 \quad q_1 \quad q_2 \quad (22)$$

With circuit swap gates interpreted as SSWAPs controlled by a parameter $\theta_k \in \mathbb{R}$. The central circuit reports a solution with $\theta_0 = \pi/2$, however adding another swap ($q_1 \rightarrow q_2$) as depicted on the right-hand side does not alter the hardware cost function, consequently the partial derivative corresponding to the second swap is zero for any $\theta_1 \in \mathbb{R}$.

In other words, there may exist configurations of the parameters vector $\boldsymbol{\theta}$ such that one or more elements of such vector determine a flat cost. However, the objective of the optimization problem (20), being a cardinality, favors the zero value for the free parameters.

△

⁵The cardinality of a vector $\mathbf{x} \in \mathbb{R}^n$ is defined as $\mathbf{card}(\mathbf{x}) := |\{i | x_i \neq 0\}|$, where $|\cdot|$ is the set cardinality.

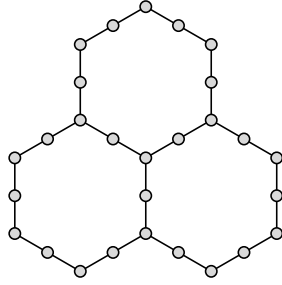


Figure 7: IBM’s heavy-hex lattice topology. The graph depicts three unit cells, with vertices representing the qubits, and edges the connectivity constraints.

3.3 The optimization problem: constraint specification for different topologies

In the construction of the hardware cost function \mathcal{L} , we claimed that the sequence of PSSWAPs in (19b) depends on some hyper-parameters. In the present section we determine the structure of the PSSWAPs for the case of the line connectivity between qubits. Despite the simplicity of the present topology, the results obtained here are key for the generalization to the arbitrary connectivity. In relation to general topologies, we notice that recently there have been a widespread adoption of quantum processing unit topologies based on hexagonal lattices [15]. An example is depicted in Figure 7. Moreover, the results obtained in this section are extend to the general case in Appendix A.1.

The line connectivity model is defined as a chain of m qubits (assuming $m \geq 3$) where the neighborhoods of qubit $k \in [1..m-2]$ are qubits $k-1$ and $k+1$. The extremes of the chain, that is qubits 0 and $m-1$, have neighborhood, respectively, qubit 1 and qubit $m-2$.

Assume for simplicity that the number of qubits m is an odd integer greater than two. Then the set of generating swaps $\mathcal{P}_{\mathcal{M}}$ defined in (14), contains $m-1$ elements. We partition the set $\mathcal{P}_{\mathcal{M}}$ into the following subsets

$$\begin{aligned}\Gamma_1 &= \{\text{SWAP}(2k, 2k+1) | k \in [0..(m-1)/2]\}, \\ \Gamma_2 &= \{\text{SWAP}(2k+1, 2k+2) | k \in [0..(m-1)/2]\},\end{aligned}\tag{23}$$

so $\mathcal{P}_{\mathcal{M}} = \Gamma_1 \cup \Gamma_2$. We note that for any $Q_1, Q_2 \in \Gamma_1$, then $Q_1 Q_2 = Q_2 Q_1$, similarly it also holds for Γ_2 .

The next lemma extends the commutativity from the generating permutations to the generated DSM. The result is immediate, so we state the claim without proof.

Lemma 3.4. *Let P_1, P_2 be $m \times m$ permutation matrices such that $P_1 P_2 = P_2 P_1$, that is the permutations commute. Then the following doubly stochastic matrices⁶ also commute*

$$Q_k = (1 - \alpha_k) \mathbb{I}_m + \alpha_k P_k,\tag{24}$$

with $\alpha_k \in [0, 1]$, for $k = 1, 2$. That is, $Q_1 Q_2 = Q_2 Q_1$.

Consequently, the product of doubly stochastic matrices obtained from either Γ_1 or Γ_2 commute. Using (16b) we define the composition of such commuting matrices (PSSWAPs) controlled

⁶Equivalent to the SSWAP defined in (15a), or the PSSWAP defined in (16a).

by the continuous parameters $\boldsymbol{\theta}$, so

$$C(\Gamma_k, \boldsymbol{\theta}) = \prod_{P_i \in \Gamma_k} (\mathbb{I}_m^{\otimes 2} + \sin^2(\theta_i) (P_i^{\otimes 2} - \mathbb{I}_m^{\otimes 2})) . \quad (25)$$

To complete the construction, we specialize the definition of $P^{(t)}$ related to the hardware cost function in (19b), with a (finite) sequence of alternating structures of the form $C(\Gamma_k, \boldsymbol{\theta})$, that is

$$P^{(t)} = C(\Gamma_1, \boldsymbol{\theta}_1^{(t)}) \cdot C(\Gamma_2, \boldsymbol{\theta}_2^{(t)}) \cdot C(\Gamma_1, \boldsymbol{\theta}_3^{(t)}) \cdot C(\Gamma_2, \boldsymbol{\theta}_4^{(t)}) \cdots \quad (26)$$

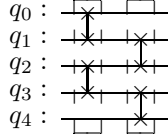


Figure 8: Example of the pattern of swaps for the line connectivity with $m = 5$ qubits. The dashed frames represent respectively the set Γ_1 and Γ_2 .

The next lemma shows one of the motivations that justify this construction, that is efficient matrix multiplication for permutations within the same partition.

Lemma 3.5. *Let $a, b \in \mathcal{S}_m$ be distinct, involutory and commuting elements of the symmetric group of degree m , that is $a \neq b$, $a^2 = b^2 = e$ and $a \circ b = b \circ a$, where $e \in \mathcal{S}_m$ is the identity element. Let P_a, P_b be the permutation representations [16] of a and b , respectively. Then*

$$P_a P_b = P_a + P_b - \mathbb{I}_m. \quad (27)$$

Proof in Appendix A.2. As a corollary, it can be readily proven that given a (finite) non-empty set of n , $m \times m$ permutation matrices $\{P_t\}_{t=1}^n$, in which each pair of elements P_a, P_b , fulfills the conditions of the Lemma, then

$$\prod_{t=1}^n P_t = \left(\sum_{t=1}^n P_t \right) - (n-1) \mathbb{I}_m. \quad (28)$$

We also note that the maximum number of disjoint and thus commuting permutation matrices is $n = \lfloor m/2 \rfloor$.

The next step is that of applying the latest result to a product of doubly stochastic matrices whose generating permutations fulfill the conditions of Lemma 3.5.

Proposition 3.6. *Let $\{P_t\}_{t=1}^n$ be a non-empty set of $m \times m$ matrices such that each element is involutory and each pair commutes. Then the following identity holds for the composition of elementary DSM generated by the P_t ,*

$$\prod_{t=1}^n (\mathbb{I}_m + \sin^2(\theta_t) (P_t - \mathbb{I}_m)) = \mathbb{I}_m + \sum_{t=1}^n \sin^2(\theta_t) (P_t - \mathbb{I}_m) . \quad (29)$$

Proof in Appendix A.2. Finally we apply the results just obtained to the definition of layer of PSSWAPs (25), so

$$C(\Gamma_k, \boldsymbol{\theta}) = \mathbb{I}_m^{\otimes 2} + \sum_{P_i \in \Gamma_k} \sin^2(\theta_i) (P_i^{\otimes 2} - \mathbb{I}_m^{\otimes 2}) . \quad (30)$$

Assume we have m qubits, then it can be shown that the repetition of patterns constructed as depicted in Figure 8, generates a set of permutations that contains a subgroup of the symmetric group \mathcal{S}_m . Also as one may expect, increasing the number of replica creates subgroups that approach in term of order, the group \mathcal{S}_m . So, it would be interesting obtaining results regarding the required number of repetitions and their efficiency. For now however, we do not expand the latter point which will be addressed in future research. To conclude, we claim without proving that this construction favors the minimization of the resulting circuit depth. However, evidence for the latter assertion emerges in the experiments section.

3.4 The optimization problem: numerical method

In this section we develop a heuristic for the solution of problem (20). We start from a well-known technique called Rolling Horizon (RH). The latter consists of partitioning a decision problem into a sequence of sub-problems whose aggregated solutions constitute a solution for the whole problem. The sub-problems often are identified by time windows of fixed length. Examples of the aforementioned strategy can be found in [12, 6].

We build on the RH strategy to obtain a process we call *adaptive feasibility*. The terminology finds the following motivation – we call it adaptive because the RH depth adjusts to the best sub-problem where we can reach feasibility. Considering the structure of the hardware cost function, we note that for all s , the variables $\theta_s^{(\tau)}$, appear in the terms \mathcal{L}_t of (18) with $t \geq \tau$. Since the permutation at time t influences the permutations of the subsequent layers, then we favor the feasibility of lower layers (w.r.t. time t) using the decreasing function $\beta(t)$ introduced in (19a). Now, it follows from Proposition 3.2 that the optimization problem takes the equivalent form

$$\begin{aligned} \min_{\boldsymbol{\theta} \in \mathbb{R}^{ST}} \|\boldsymbol{\theta}\|_2^2, \\ \text{s.t. } \mathcal{L}(\boldsymbol{\theta}) = 0, \end{aligned}$$

which we solve using the *Differential Multiplier Method* [14]. The method, by introducing the Lagrange multiplier λ , produces a sequence of updates for the variables $\boldsymbol{\theta}$ and λ , so

$$\boldsymbol{\theta} \leftarrow \boldsymbol{\theta} - \eta_\theta \nabla_\theta \left(\|\boldsymbol{\theta}\|_2^2 + \lambda \mathcal{L}(\boldsymbol{\theta}) \right), \quad (31a)$$

$$\lambda \leftarrow \lambda + \eta_\lambda \nabla_\lambda \left(\|\boldsymbol{\theta}\|_2^2 + \lambda \mathcal{L}(\boldsymbol{\theta}) \right), \quad (31b)$$

until a stop condition is reached. We denoted with η_θ and η_λ the step sizes for the variables $\boldsymbol{\theta}$ and λ , respectively. Interestingly, since $\mathcal{L}(\boldsymbol{\theta}) \geq 0$, the second update corresponds to a monotonic increase of λ , that is

$$\lambda \leftarrow \lambda + \eta_\lambda \mathcal{L}(\boldsymbol{\theta}). \quad (32)$$

The latter can be used to prove that the optimizer gets attracted by the stationary points of \mathcal{L} , but according to Proposition 3.3, such points have a known and convenient structure.

The entire procedure is split into two algorithms, the DSM-SWAP and the Knitter, with the former being the main algorithm.

3.4.1 The Knitter algorithm

The Knitter⁷ algorithm can be interpreted as a global solver (w.r.t. the circuit) for the swap mapping problem. But the input circuit is split into sections using the RH strategy so the Knitter only acts upon each of the sub-circuits separately.

⁷The name Knitter is inspired by the braid diagrams (Figure 9) used to represent the iteration of the SWAPs.

We describe the steps of the algorithm as presented in Algorithm 1. The input circuit is given as a sequence of graphs $\mathcal{G}^{(t)}$, the latter is used alongside the hardware graph \mathcal{M} to construct (function `BuildHardwareCost`) the hardware cost function \mathcal{L} . The construction depends on the machine topology, details are elaborated in sections A.1 and 3.3.

In the for-loop at line 6 the vector θ is updated in a gradient descent fashion using the gradient of the function $f(\theta) = \|\theta\|_2^2 + \lambda\mathcal{L}(\theta)$. Since the problem is non-convex, the iteration is executed `max_trials` ≥ 1 times. At the end of each iteration, the *projection*⁸ $\mathfrak{P}_{\Omega^{ST'}}$ onto the set $\Omega^{ST'}$ is applied to the vector θ , with Ω defined as in Proposition 3.3. Furthermore, the application of the projector is justified by Proposition 3.3.

Completed the trials at line 15, we use the merit function $g(\theta) = \|\theta\|_2^2 + \alpha\mathcal{L}(\theta)$ to choose the best solution⁹. Here the parameter $\alpha > 0$ is a trade-off between swaps minimization and feasibility maximization. Once the best solution is realized, at line 16 we count the number l of subsequent layers, starting from the first, that fulfill the hardware constraints. Here we denote with $\delta_{\{0\}}$ the indicator function¹⁰ for the set $\{0\} \subset \mathbb{R}$. Remarkably, line 16 constitutes one of the key elements for the adaptive feasibility. Finally the algorithm returns the sub-vector of θ^* corresponding to the first l layers.

Algorithm 1: The pseudocode for the Knitter algorithm.

```

Data: Sequence of  $T'$  circuit layers as graphs  $\mathcal{G}^{(t)}$ . Hardware connectivity graph  $\mathcal{M}$ .
Result:  $\theta^*$ ; // Parameters for the feasible layers
1  $R \leftarrow \emptyset$ ; // Set of solutions from trials
2  $\mathcal{L} \leftarrow \text{BuildHardwareCost} \left( (\mathcal{G}^{(t)})_{t=1}^{T'}, \mathcal{M} \right)$ ; // Prepare the hardware cost function
3 for  $t \leftarrow 1$  to max_trials do
4    $\theta \sim \text{U}_{ST'}(0, \epsilon)$ ; // Sample initial  $\theta \in \mathbb{R}^{ST'}$ , with  $\epsilon > 0$  a small constant.
5    $\lambda \sim \text{U}(0, \epsilon)$ ; // Sample initial  $\lambda$ . U is the uniform distribution.
6   for  $\tau \leftarrow 1$  to max_optim_steps do
7      $\theta \leftarrow \theta - \eta_\theta \nabla_\theta (\|\theta\|_2^2 + \lambda\mathcal{L}(\theta))$ ; // Update  $\theta$  with GD step
8      $\lambda \leftarrow \lambda + \eta_\lambda \mathcal{L}(\theta)$ ; // Update  $\lambda$ 
9     if  $\|\nabla_\theta \mathcal{L}(\theta)\|_2^2 \leq \gamma$  then
10      | break; // Early stopping condition met
11    end
12  end
13   $R \leftarrow R \cup \{\mathfrak{P}_{\Omega^{ST'}}(\theta)\}$ ; // Store projection of current  $\theta$ 
14 end
15  $\theta^* \leftarrow \underset{\theta \in R}{\text{argmin}} \|\theta\|_2^2 + \alpha\mathcal{L}(\theta)$ ; // Best solution selection policy
16  $l \leftarrow \underset{k \in [0..T']}{\text{argmin}} \delta_{\{0\}} \left( \sum_{i=0}^{k-1} \mathcal{L}_i(\theta^*) \right) - k$ ; // Count feasible layers in  $l$ 
17 if  $l$  is 0 then
18   | // No feasible layers
19   |  $\theta^* \leftarrow \text{nil}$ ;
20 end
21  $\theta^* \leftarrow \theta^*[1..l * S]$ ; // Select parameters (sub-vector) for the  $l$  feasible layers

```

⁸The definition of *projection* is given in the proof of Lemma A.4.

⁹In our specific implementation we choose the solution that maximizes the number of feasible layers, consequently the adaptive horizon step is maximized, leading to a reduction of the overall computation time for the method.

¹⁰The indicator function for a subset $C \subseteq U$ is defined as the extended real-valued function $\delta_C : U \rightarrow \mathbb{R} \cup \{\infty\}$ with rule $\delta_C(\mathbf{x}) = \begin{cases} 0, & \mathbf{x} \in C, \\ \infty, & \text{otherwise.} \end{cases}$

3.4.2 The DSM-SWAP algorithm

The DSM-SWAP algorithm in essence partitions the input circuit into sub-circuits upon which the `Knitter` algorithm is executed. The pseudocode is presented in Algorithm 2, also we recall that we denote with T the number of layers of the circuit and with S the number of parameters (equivalently SWAPs) per layer. The depth of the sub-circuits is given by the hyper-parameter `horizon`, however the starting point for the horizon advances adaptively (line 13) depending on the feasibility reached by the previous iteration.

Function `ThetasToSwaps` invoked at lines 6 and 16 takes a vector of angles θ to a sequence of permutations matrices. We note that the elements of the vector θ are expected to belong to the set Ω (Proposition 3.3), that is the angles represent a vertex of the Birkhoff polytope. But this is consistent with the value returned by function `Knitter`.

We remark one additional point at line 7. The permutations applied to layer t , influence all the subsequent layers from $t + 1$ to $T - 1$. Consequently, we make the algorithm consistent with the mechanism by pre-permuting the qubits of each block C with the permutations from the previous layers. In the specific expression at line 7 we denote with $(\cdot) \bullet (\cdot)$ the action of the permutation P on the circuit C .

Finally the result of the method consists of a sequence of $T \times S$ involutory permutation matrices (either identity or SWAP). In Figure 7 the reader can appreciate the resulting structure visually.

Algorithm 2: The pseudocode for the DSM-SWAP algorithm.

```

Data: Sequence of  $T$  circuit layers as graphs  $\mathcal{G}^{(t)}$ . Hardware connectivity graph  $\mathcal{M}$ .
Result:  $R$ ; // Sequences of swaps for each layer
1  $\theta^* \leftarrow ()$ ; // Init empty vector ( $\dim \theta^* = 0$ ) for the parameters
2  $t \leftarrow 0$ ;
3 while  $t < T$  do
    // Iterate over circuit layers
4      $h \leftarrow \min(\text{horizon}, T - t)$ ; // Compute effective horizon
5      $C \leftarrow (\mathcal{G}^{(\tau)})_{\tau=t}^{t+h}$ ; // Construct sub-circuit with depth up to horizon
6      $P \leftarrow \text{ThetasToSwaps}(\theta^*)$ ;
7      $C \leftarrow P \bullet C$ ; // Apply the resulting permutation up to layer  $t$ 
8      $\theta \leftarrow \text{Knitter}(C, \mathcal{M})$ ; // Run Knitter on permuted sub-circuit  $C$ 
9     if  $\theta$  is nil then
        // If there are no feasible layers
        // fail or run alternative strategy
10         $R \leftarrow \text{nil}$ ; // Nil result
11        return;
12    end
13     $t \leftarrow t + (\dim \theta) / S$ ; // Adaptively update the next horizon starting point
14     $\theta^* \leftarrow \theta^* \oplus \theta$ ; // Extend the vector of parameters
    // Note  $\dim \theta^* = t \times S \leq T \times S$ .
15 end
    // The final  $\theta^*$  belongs to  $\mathbb{R}^{ST}$ 
16  $R \leftarrow \text{ThetasToSwaps}(\theta^*)$ ; // Obtain swaps for all layers

```

4 Experiments

The purpose of the experiments is two fold. On one hand we aim at obtaining a clearer view of the effects of the hyper-parameters. On the other one, we compare the results of the proposed method with other well known algorithms in literature.

The algorithm DSM-SWAP has been implemented¹¹ on top of the frameworks Qiskit [1] and PyTorch [13]. From the Qiskit library, we also made use of the algorithm SABRE and the circuit generators for the multi-controlled X gate and Quantum Volume.

The circuits involved in the experiments may present features with different distributions, depending on patterns and number of qubits. Also the measurements we are considering are taken both before and after the application of the swap mapping process. To evaluate the generalization of the strategy we consider several circuit patterns, specifically the Quantum Volume (QV¹²) circuits [5] and the multi-cX gates compiled with an alphabet consisting of CNOT and single qubit gates. Given a circuit pattern C and a feature X , we denote with $X_0(C)$ and $X_s(C)$ the random variables for the feature X measured on C , respectively before and after the swap mapping. Then given the samples $x_0 \sim X_0(C)$ and $x_s \sim X_s(C)$, assuming $x_0 \neq 0$, we define the relative measure as $d = \frac{x_s - x_0}{x_0}$. The features we consider are the number of CNOTs and the circuit depth¹³. The features are computed on the circuit resulting from the invocation of the Qiskit¹⁴ transpiler with optimization level three¹⁵. We note that the transpiler embodies algorithms based on the stochastic approach, thus modeling using random variables is justified. Take for example the number of CNOTs and let c_0, c_s be their count before and after the swap mapping. Then the relative measure $\text{dcnots} = \frac{c_s - c_0}{c_0}$ represents the fractional increase in the number of CNOTs as a result of the qubit allocation. So for example, if the circuit prior to the swap mapping contains 100 CNOTs and the process produces a fractional increase of 0.75 units ($\text{dcnots} = 0.75$), then the final circuits contains 175 CNOTs. Similarly we denote the fractional increase in depth with ddepth .

4.1 Study of the hyper-parameters

We start by describing the structure of the sampling. We generate 250 QV circuit instances for each qubit count from 5 to 8 (both inclusive). Each circuit instance is then processed by the DSM-SWAP algorithm configured with combinations of increasing horizon $\{1, 2, 4\}$ and maximum optimizer steps $\{10, 30, 100\}$.

In Figure 10 we highlight the general positive effect of a longer horizon on both dcnots and ddepth . Moreover, Figure 9 provides the same evidence using braid diagrams. In Figure 11 we observe vague evidence that a higher number of steps increases the quality of the results. This means that the optimizer converges quite fast so we conclude that there is not much difference between 30 and 100 steps, thus the former value is set as the default.

4.2 DSM-SWAP vs SABRE

We compare the new method with the algorithm SABRE configured with the lookahead strategy [8]. The circuits considered are the Quantum Volume and the multi-cX gates. The data for DSM-SWAP is the same one obtained for the hyper-parameters investigations¹⁶ we denote the corresponding features with dcnots_{dsm} and ddepth_{dsm} . In addition we execute SABRE on the same circuits and measure the features dcnots_{sabre} and ddepth_{sabre} . In Figures 12 and 13, we

¹¹Source code available at <https://github.com/qiskit-community/dsm-swap>.

¹²In the interest of space, we denote with $\text{QV}\{n\}$ a Quantum Volume circuit with n qubits. Moreover, the latter is generated via the function `qiskit.circuit.quantumcircuit.QuantumCircuit(n, seed=seed)`, where `seed` determines the circuit instance.

¹³We consider the Qiskit [1] definition of circuit depth which can be obtained through the method `qiskit.circuit.QuantumCircuit.depth`.

¹⁴Qiskit 0.36.1 and Qiskit Terra 0.20.1.

¹⁵Specifically, the structure of the invocation is `qiskit.compiler.transpile(..., optimization_level=3)`.

¹⁶We fix the hyper-parameter `max_optim_steps = 30`.

plot the eCDFs for the features gaps

$$\text{dcnots} = \text{dcnots}_{\text{sabre}} - \text{dcnots}_{\text{dsm}} \quad (33a)$$

$$\text{ddepth} = \text{ddepth}_{\text{sabre}} - \text{ddepth}_{\text{dsm}}. \quad (33b)$$

Since the selected features, the smaller they are the better the performance, then points on the positive abscissa correspond to DSM-SWAP performing better than SABRE. In Figure 12 we see that for `horizon` ≥ 2 , the new method has at least 80% chances to produce a shallower circuit. In Figure 13 we distinguish the results for QV8 circuits assuming line and ring couplings. Surprisingly, in the ring connectivity case, the gap is remarkable even for `horizon` = 1. We think that the latter could be an important clue for the development of new swap mapping methods.

In Figure 15 we obtain the average values for the merit measure defined as

$$\text{merit} = \text{dcnots} + \text{ddepth}, \quad (34)$$

which can be interpreted as the overall increase in both CNOT count and depth, as a consequence of the swap mapping. The latter figure shows how our method compares to SABRE as the `horizon` increases, also we consider MCX and QV8 circuits.

Remark 4.1. We expand on the reason for the choice of QV and MCX circuits. The Quantum Volume circuits have the property that each layer is represented by a graph $\mathcal{G}^{(t)}$ that has the maximum number of edges such that the corresponding two-qubit gates commute. This feature can be appreciated in Figure 9 by observing the columns (layers) of red edges.

On the other hand, MCX circuits, compiled with an alphabet of CNOT and single qubit gates, present layers that tend to have a single edge, consequently they represent the opposing case to QV.

△

Following the previous remark we assert that the case of the QV circuits is the most advantageous for DSM-SWAP since the construction of the SWAPs (Sections 3.3 and A.1) can maximize the parallelism of the permutations. The MCX circuits instead should be the opposing case, indeed we observe in Figure 15 that we need a longer horizon to obtain a neat advantage over SABRE.

5 Conclusions

The swap mapping process is fundamental for the quantum compiler and increasing its efficiency is essential for improving the performance of the hardware. In this work we obtained a procedure that combines both mathematical optimization and heuristic strategies. In literature however, methods based on mathematical optimization have not recorded particular successes when applied to this problem. Conscious of the computation complexity hardness of the problem we understand that, to be practical, the algorithm must include an heuristic component.

The decision process for the insertion of the SWAPs has been modeled as a smooth optimization based on doubly stochastic matrices. Also we obtained a procedure to build the pattern of SWAPs depending on the topology of the target hardware. One of the bottlenecks in the evaluation of the cost function is determined by the number of matrix multiplications, however, using the commutativity properties of the pattern we devised an efficient scheme for reducing the computational cost. The solver heuristic is inspired by the rolling horizon policy and it offers linear scaling of the computational complexity with respect to the depth of the circuit. The algorithm has been implemented on top of the frameworks Qiskit and PyTorch, also we

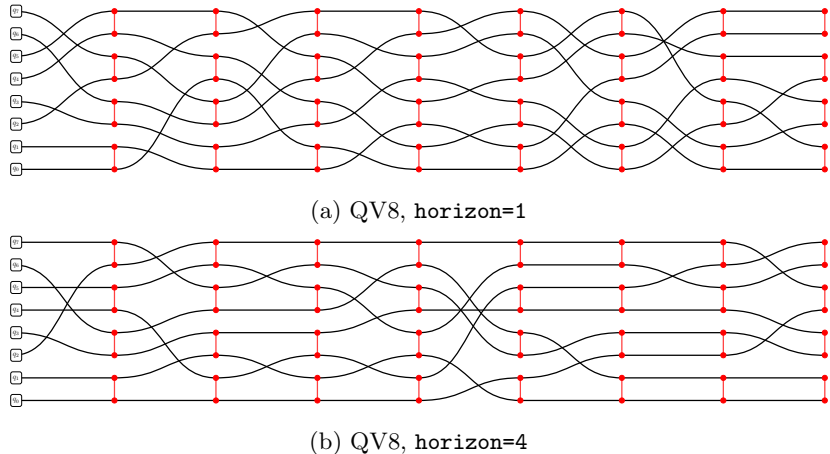


Figure 9: *Braid diagrams* for the swap mapping applied to a Quantum Volume circuit with 8 qubits. The results, starting from the top, correspond to respectively horizon 1 and 4. It can be noticed that in the bottom case the density of the braids (permutations) is visibly lower.

made the code open source. The experiments revealed clues regarding the algorithm hyper-parameters and its relation with the state of the art algorithm SABRE. The optimality of the results has been measured using the relative increment in CNOT gate count and depth. For the hyper-parameters, we found that an increased horizon for the adaptive feasibility influences positively the performance of the results. The comparison with the algorithm SABRE shown that at the cost of increased computational time and while preserving the number of CNOTs, the new method delivers significant reduction in the depth of the resulting circuit. We see the potential application of our method to the compiling of quantum libraries where the processing time can be penalized in favor of depth and CNOTs optimality.

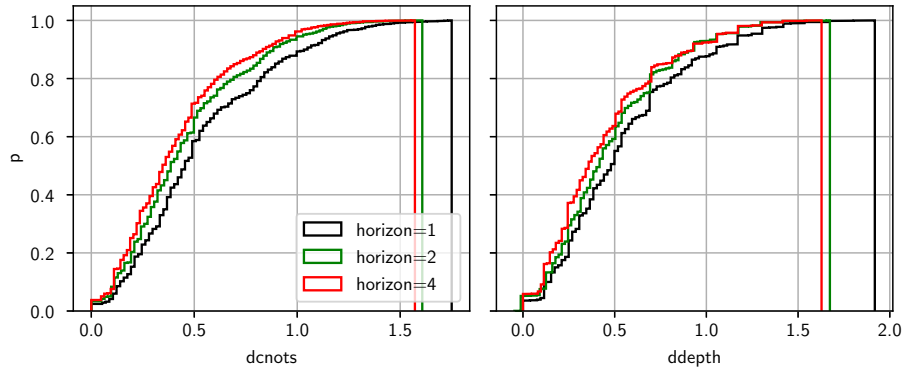
Despite the positive results, further research is required to extend the applicability of the method to the upcoming quantum hardware where we expect the number of qubits to climb to hundreds if not thousands.

Acknowledgment

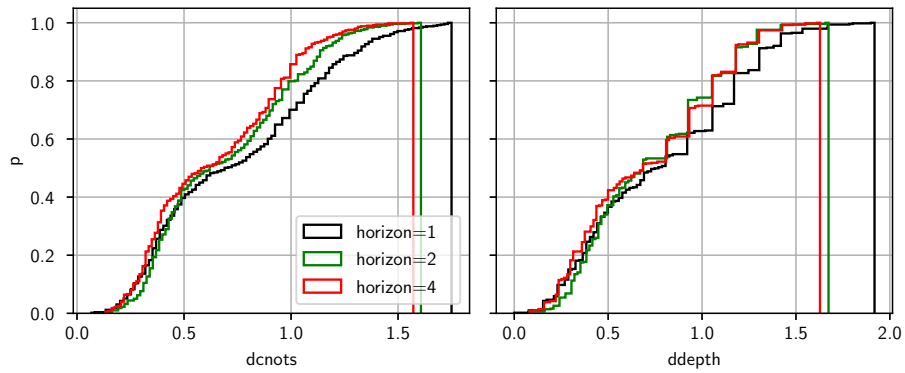
This study has received funding from the Disruptive Technologies Innovation Fund (DTIF), by Enterprise Ireland, under project number DTIF2019-090 (project QCoIR). The literature review is based on some unpublished work by Claudio Gambella, Andrea Simonetto, Anton Dekusar and Giacomo Nannicini. The open source implementation was realized thanks to the collaboration of Anton Dekusar, Albert Akhriev and Kevin Krsulich. The authors are highly thankful to Ali Javadi-Abhari, Dr. Martin Mevissen and Tara Murphy for their support and suggestions.

References

- [1] Qiskit: An open-source framework for quantum computing, 2021.
- [2] Amir Beck. *First-Order Methods in Optimization*. SIAM-Society for Industrial and Applied Mathematics, Philadelphia, PA, USA, 2017.

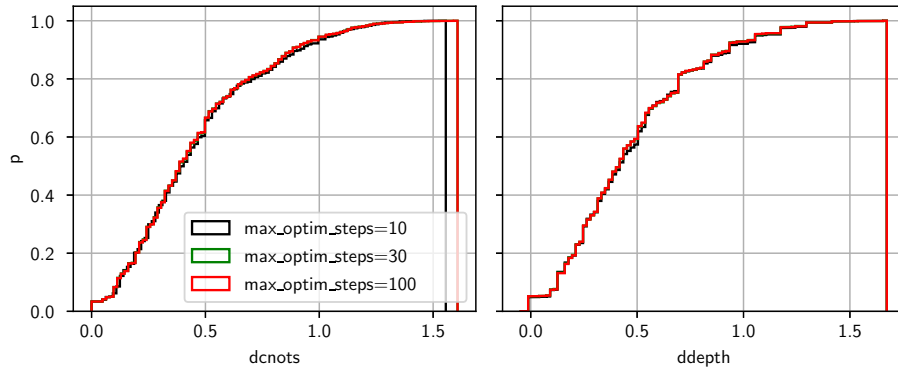


(a) QV{5, 6, 7, 8}

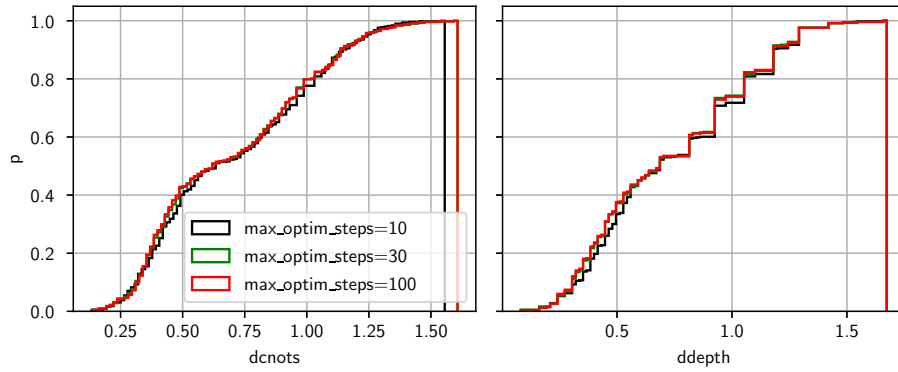


(b) QV8

Figure 10: The eCDFs for features `dcnots` (left column) and `ddepth` (right column) measured on the algorithm DSM-SWAP. The top row configuration consists of increasing horizon (`horizon = 1, 2, 4`) over QV{5, 6, 7, 8} circuits and maximum optimizer steps fixed to 30. The bottom row corresponds to the same configuration, however it relates exclusively to the QV8 circuits.



(a) QV{5, 6, 7, 8}



(b) QV8

Figure 11: The eCDFs for features `dcnots` (left column) and `ddepth` (right column) measured on the algorithm DSM-SWAP. The top row configuration consists of increasing maximum optimizer steps (`max_optim_steps = 10, 30, 100`) over QV{5, 6, 7, 8} circuits and horizon fixed to 2. The bottom row corresponds to the same configuration, however it relates exclusively to the QV8 circuits.

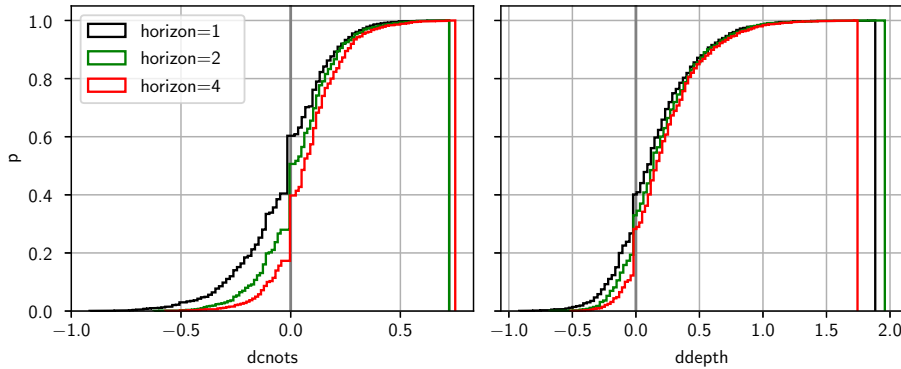
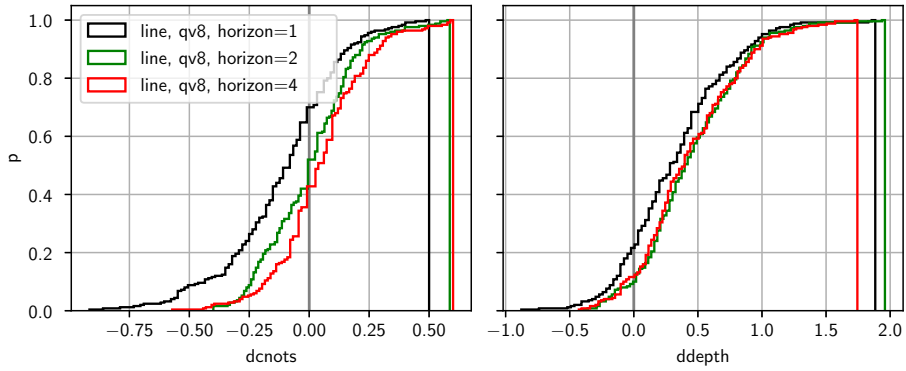
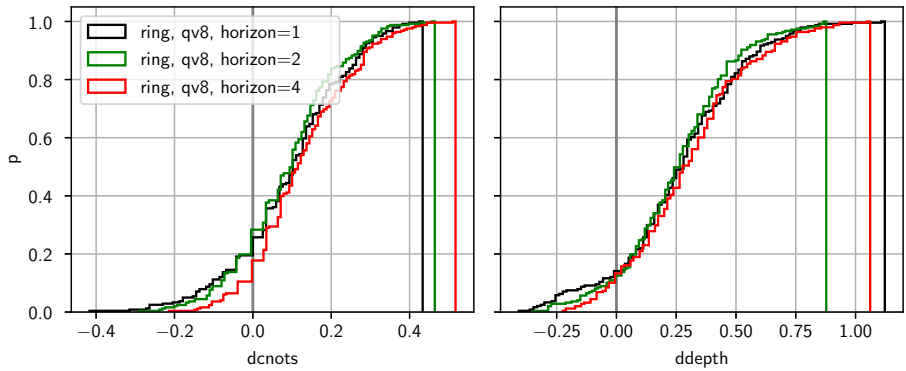


Figure 12: The eCDFs for features gap `dcnots` (left) and `ddepth` (right) for the comparative case DSM-SWAP vs SABRE. The DSM-SWAP algorithm is configured with increasing horizon (`horizon = 1, 2, 4`) and `max_optim_steps = 30`. The vertical gray line at abscissa zero determines the threshold where the two algorithms produce the same result (w.r.t. the current feature), whereas on the right-hand side, the DSM-SWAP yields more favorable results.

- [3] Richard A. Brualdi. *Combinatorial Matrix Classes*. Encyclopedia of Mathematics and its Applications. Cambridge University Press, 2006.
- [4] Gavin E. Crooks. Gradients of parameterized quantum gates using the parameter-shift rule and gate decomposition. 2019.
- [5] Andrew W. Cross, Lev S. Bishop, Sarah Sheldon, Paul D. Nation, and Jay M. Gambetta. Validating quantum computers using randomized model circuits. *Physical Review A*, 100(3), sep 2019.
- [6] Claudio Gambella, Enrico Malaguti, Filippo Masini, and Daniele Vigo. Optimizing relocation operations in electric car-sharing. *Omega*, 81:234–245, 2018.
- [7] Roger A. Horn and Charles R. Johnson. *Matrix Analysis*. Cambridge University Press, USA, 2nd edition, 2012.
- [8] Gushu Li, Yufei Ding, and Yuan Xie. Tackling the qubit mapping problem for nisq-era quantum devices. In *Proceedings of the Twenty-Fourth International Conference on Architectural Support for Programming Languages and Operating Systems*, pages 1001–1014, 2019.
- [9] Easwar Magesan, Jay M. Gambetta, and Joseph Emerson. Characterizing quantum gates via randomized benchmarking. *Physical Review A*, 85(4), apr 2012.
- [10] Dmitri Maslov, Sean M Falconer, and Michele Mosca. Quantum circuit placement. *IEEE Transactions on Computer-Aided Design of Integrated Circuits and Systems*, 27(4):752–763, 2008.
- [11] Giacomo Nannicini, Lev S Bishop, Oktay Gunluk, and Petar Jurcevic. Optimal qubit assignment and routing via integer programming, 2021.
- [12] Rodrigo Palma-Behnke, Carlos Benavides, Fernando Lanas, Bernardo Severino, Lorenzo Reyes, Jacqueline Llanos, and Doris Sáez. A microgrid energy management system based on the rolling horizon strategy. *IEEE Transactions on Smart Grid*, 4(2):996–1006, 2013.



(a) QV8-line



(b) QV8-ring

Figure 13: The same experiment as that in Figure 12 except that here we distinguish the case with QV8 circuits with line (top row) and ring (bottom row) coupling maps.

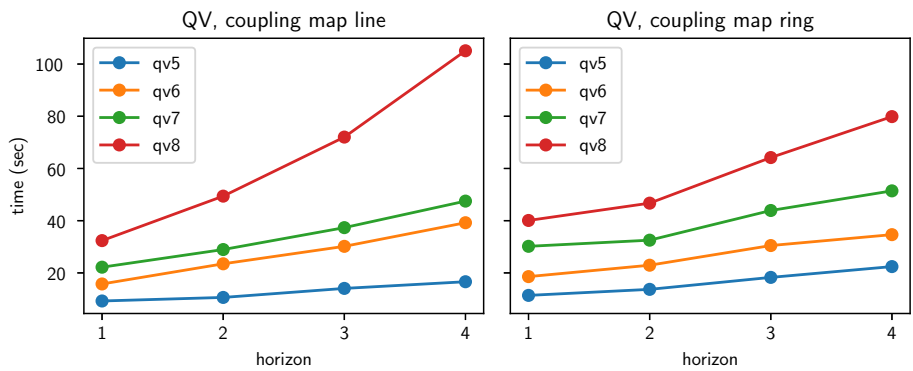


Figure 14: Average time for the DSM-SWAP obtained at increasing horizon with QV circuits.

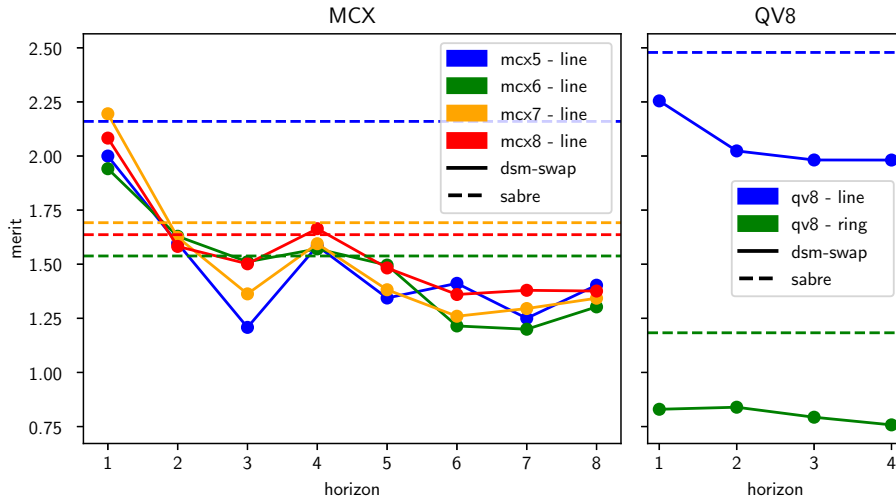


Figure 15: Comparison DSM-SWAP vs SABRE w.r.t. the merit function defined in (34), on MCX (left) and QV8 (right) circuits.

- [13] Adam Paszke, Sam Gross, Francisco Massa, Adam Lerer, James Bradbury, Gregory Chanan, Trevor Killeen, Zeming Lin, Natalia Gimelshein, Luca Antiga, Alban Desmaison, Andreas Kopf, Edward Yang, Zachary DeVito, Martin Raison, Alykhan Tejani, Sasank Chilamkurthy, Benoit Steiner, Lu Fang, Junjie Bai, and Soumith Chintala. Pytorch: An imperative style, high-performance deep learning library. In H. Wallach, H. Larochelle, A. Beygelzimer, F. d'Alché-Buc, E. Fox, and R. Garnett, editors, *Advances in Neural Information Processing Systems 32*, pages 8024–8035. Curran Associates, Inc., 2019.
- [14] John Platt and Alan Barr. Constrained differential optimization. In D. Anderson, editor, *Neural Information Processing Systems*, volume 0. American Institute of Physics, 1987.
- [15] IBM Quantum. The ibm quantum heavy hex lattice. Available at <https://research.ibm.com/blog/heavy-hex-lattice> (2021/07/07).
- [16] Bruce E. Sagan. *The Symmetric Group: Representations, Combinatorial Algorithms, and Symmetric Functions*. Springer New York, New York, NY, 2001.
- [17] Marcos Yukio Siraichi, Vinicius Fernandes Dos Santos, Caroline Collange, and Fernando Magno Quintão Pereira. Qubit Allocation. In *CGO 2018 - International Symposium on Code Generation and Optimization*, pages 1–12, Vienna, Austria, February 2018.
- [18] Bochen Tan and Jason Cong. Optimality study of existing quantum computing layout synthesis tools. *IEEE Transactions on Computers*, 70(9):1363–1373, sep 2021.
- [19] V. G. Vizing. Critical graphs with given chromatic class. *Metody Diskret. Analiz.*, 5:9–17, 1965.

A Appendix

A.1 Arbitrary topology

We extend the results obtained in the previous section from line connectivity to arbitrary topology. The disjoint partitioning $\mathcal{P}_{\mathcal{M}} = \Gamma_1 \cup \Gamma_2$ of the set of generating swaps, obtained in (23), can be interpreted as a special case of the *graph edge coloring problem*. In Figure 16 we provide an example of line connectivity related to the partitioning and its relation to edge coloring.

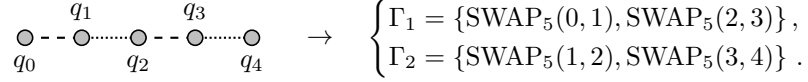


Figure 16: An example of edge coloring for the line connectivity. On the LHS we have the graph \mathcal{M} with the line pattern representing the color of the edge. On the RHS we have the partitions obtained in (23).

We recall that the m swap targets i, j for each swap $\text{SWAP}_m(i, j) \in \mathcal{P}_{\mathcal{M}}$, and the swaps in $\mathcal{P}_{\mathcal{M}}$, correspond respectively to the vertices and the edges of the hardware connectivity graph \mathcal{M} . Then the minimum number of partitions of \mathcal{M} , such that no two incident edges are in the same subset, is called the *edge chromatic index*. For a graph \mathcal{G} we denote its chromatic index with $\chi_e(\mathcal{G})$. Therefore the optimal partitions Γ_k correspond to the colors in the edge coloring problem. An example for this general case is provided in Figure 17.

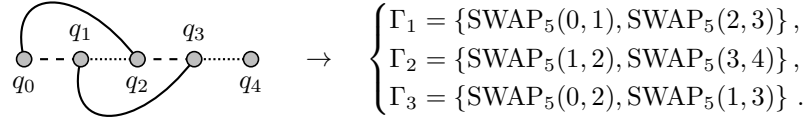


Figure 17: An example of edge coloring and the corresponding partitioning of the generators set. On the LHS we have the graph \mathcal{M} with the line pattern representing the color of the edge.

Assume that the hardware graph \mathcal{M} corresponds to an arbitrary topology. Then, by applying the edge coloring procedure, we determine the optimal partitioning

$$\mathcal{P}_{\mathcal{M}} = \bigcup_{k=1}^{\chi_e(\mathcal{M})} \Gamma_k, \quad (35)$$

such that fixed any $k \in [1 \dots \chi_e(\mathcal{M})]$, we have that $P_a, P_b \in \Gamma_k$ implies $P_a P_b = P_b P_a$.

Given the max degree of a graph \mathcal{G} , denoted by $\Delta(\mathcal{G})$, a well known result by Vizing [19] establishes the boundaries for its chromatic index. We report the aforementioned theorem.

Proposition A.1 (Vizing). *Given any finite and simple graph \mathcal{G} , then $\Delta(\mathcal{G}) \leq \chi_e(\mathcal{G}) \leq \Delta(\mathcal{G}) + 1$.*

In other words we need at most $\Delta(\mathcal{M}) + 1$ subsets for the partitioning of $\mathcal{P}_{\mathcal{M}}$.

In relation to the heavy-hex lattice topology depicted in Figure 7, we notice that graphs of such form are planar and have maximum degree 3. Consequently, by Theorem A.1, a hexagonal lattice connectivity requires not more than 4 partitions.

A.2 Proofs

Proof of Lemma 2.2. The first equality follows immediately from the definitions of $\text{vec}_r(\mathbb{I}_n)$ and $\text{vec}_r(A)$. For the second one, consider the decomposition $A = \sum_{i,j} A_{i,j} |i\rangle_n \langle j|_n$, then

$$(\mathbb{I}_n \otimes A^\top) \text{vec}_r(\mathbb{I}_n) = \left(\mathbb{I}_n \otimes \sum_{i,j} A_{i,j} |j\rangle_n \langle i|_n \right) \sum_k |k\rangle_n \otimes |k\rangle_n \quad (36a)$$

$$= \sum_{i,j} (|i\rangle_n \otimes (A_{i,j} |j\rangle_n)) = \text{vec}_r(A). \quad (36b)$$

□

Proof of Lemma 2.3. We prove the equality between the left-hand side (LHS) of (5a) and (5b), so

$$\text{vec}_r(\mathbb{I}_n)^\top (A \otimes B) \text{vec}_r(\mathbb{I}_n) = \left(\sum_i \langle i| \otimes \langle i| \right) (A \otimes B) \left(\sum_j |j\rangle \otimes |j\rangle \right) \quad (37a)$$

$$= \sum_{i,j} \langle i| A |j\rangle \otimes \langle i| B |j\rangle \quad (37b)$$

$$= \sum_{i,j} A_{i,j} B_{i,j} = \mathbf{1}_n^\top (A \odot B) \mathbf{1}_n. \quad (37c)$$

Using Lemma 2.2, we prove the trace identity. First note that, for some $i, j \in [0..n-1]$, $|j\rangle \otimes (\langle i| \mathbb{I}_n |j\rangle) = |i\rangle$ when $i = j$ and 0 otherwise. Then

$$\text{Tr}(AB^\top) = \sum_{i=0}^{n-1} \langle i| AB^\top |i\rangle \quad (38a)$$

$$= \sum_{i,j=0}^{n-1} \langle i| AB^\top |j\rangle \otimes \langle i| \mathbb{I}_n |j\rangle \quad (38b)$$

$$= \text{vec}_r(\mathbb{I}_n)^\top (AB^\top \otimes \mathbb{I}_n) \text{vec}_r(\mathbb{I}_n) \quad (38c)$$

$$= \text{vec}_r(\mathbb{I}_n)^\top (A \otimes \mathbb{I}_n) (B^\top \otimes \mathbb{I}_n) \text{vec}_r(\mathbb{I}_n) \quad (38d)$$

$$\stackrel{(4)}{=} \text{vec}_r(\mathbb{I}_n)^\top (A \otimes \mathbb{I}_n) (\mathbb{I}_n \otimes B) \text{vec}_r(\mathbb{I}_n) \quad (38e)$$

$$= \text{vec}_r(\mathbb{I}_n)^\top (A \otimes B) \text{vec}_r(\mathbb{I}_n). \quad (38f)$$

□

Proof of Lemma 3.1. Since Q is doubly stochastic, then $\sum_i \lambda_i = 1$ and $\lambda_i \geq 0$. We verify the Definition 1, so

$$K(J_m \otimes J_m) = \left(\sum_i \lambda_i P_i \otimes P_i \right) (J_m \otimes J_m) \quad (39a)$$

$$= \sum_i \lambda_i (P_i J_m) \otimes (P_i J_m) \quad (39b)$$

$$= \left(\sum_i \lambda_i \right) J_m \otimes J_m = J_m \otimes J_m. \quad (39c)$$

Similarly, it can be proved for the left-hand side multiplication by $J_m \otimes J_m$. Thus $K(J_m \otimes J_m) = (J_m \otimes J_m)K = J_m \otimes J_m$, hence the implication follows. \square

Lemma A.2. *The partial derivatives of the hardware cost function (18) w.r.t. $\theta_s^{(t)}$, follow the parameter shift rule [4], that is*

$$\frac{\partial \mathcal{L}(\boldsymbol{\theta})}{\partial \theta_s^{(t)}} = \mathcal{L}\left(\boldsymbol{\theta} + \frac{\pi}{4} \mathbf{e}_s^{(t)}\right) - \mathcal{L}\left(\boldsymbol{\theta} - \frac{\pi}{4} \mathbf{e}_s^{(t)}\right), \quad (40)$$

where $\mathbf{e}_s^{(t)}$ is the standard basis vector whose index is (t, s) .

Proof. First note that

$$\frac{\partial \sin^2(\theta)}{\partial \theta} = 2 \sin \theta \cos \theta = \sin(2\theta) \quad (41a)$$

$$= \left(\frac{1}{2} + \frac{1}{2} \sin(2\theta)\right) - \left(\frac{1}{2} - \frac{1}{2} \sin(2\theta)\right) \quad (41b)$$

$$= \left(\frac{1}{2} - \frac{1}{2} \cos\left(2\theta + \frac{\pi}{2}\right)\right) - \left(\frac{1}{2} - \frac{1}{2} \sin\left(2\theta - \frac{\pi}{2}\right)\right) \quad (41c)$$

$$= \sin^2\left(\theta + \frac{\pi}{4}\right) - \sin^2\left(\theta - \frac{\pi}{4}\right). \quad (41d)$$

Consider the matrix-valued function $\text{SSWAP}_m(\cdot; i, j) : \mathbb{R} \rightarrow \mathcal{M}_m$, then fixed some $\mathbf{v}, \mathbf{w} \in \mathbb{R}^m$, we have

$$\frac{\partial (\mathbf{v}^\top \text{SSWAP}_m(i, j, \theta) \mathbf{w})}{\partial \theta} = \frac{\partial \sin^2(\theta)}{\partial \theta} (\mathbf{v}^\top \text{SWAP}_m(i, j) \mathbf{w} - \mathbf{v}^\top \mathbf{w}) \quad (42a)$$

$$= \mathbf{v}^\top \text{SSWAP}_m\left(i, j, \theta + \frac{\pi}{4}\right) \mathbf{w} - \mathbf{v}^\top \text{SSWAP}_m\left(i, j, \theta - \frac{\pi}{4}\right) \mathbf{w}, \quad (42b)$$

and similarly for PSSWAP. But the LHS of (42a) corresponds to the form of $\frac{\partial \mathcal{L}_t(\boldsymbol{\theta})}{\partial \theta_s^{(t)}}$. Also, since the variables $\theta_s^{(t)}$ appear not more than once in each term of the cost in (18) then by linearity the result follows. \square

Lemma A.3. *Let Q be an $m \times m$ DSM, then the ℓ_1 -norm of vectors from the non-negative orthant \mathbb{R}_+^m is preserved under the action of Q . That is*

$$\mathbf{v} \in \mathbb{R}_+^m \implies \|Q\mathbf{v}\|_1 = \|\mathbf{v}\|_1, \quad (43)$$

for all $m \times m$ DSMs Q .

Proof. Since $\mathbf{v} \in \mathbb{R}_+^m$, so each component v_i is non-negative, then the ℓ_1 -norm can be written as $\|\mathbf{v}\|_1 = \mathbf{1}_m^\top \mathbf{v}$. Note that for any $m \times m$ permutation matrix P , we have $P\mathbf{1}_m = \mathbf{1}_m$. Let $Q = \sum_j \lambda_j P_j$ be any $m \times m$ DSM, where λ_j and P_j follow Definition 1. Hence

$$\|Q\mathbf{v}\|_1 = \left\| \sum_j \lambda_j P_j \mathbf{v} \right\|_1 = \sum_j \lambda_j \mathbf{1}_m^\top P_j \mathbf{v} \quad (44a)$$

$$= \mathbf{1}_m^\top \mathbf{v} \sum_j \lambda_j = \|\mathbf{v}\|_1, \quad (44b)$$

consequently the claim is proved. \square

Proof of Proposition 3.3. From Lemma A.2 and the structure of the function \mathcal{L} , it follows that the partial derivative w.r.t. $\theta_s^{(t)}$ takes the form

$$\begin{aligned} \frac{\partial \mathcal{L}(\boldsymbol{\theta})}{\partial \theta_s^{(t)}} &= \sum_{\tau=t}^{T-1} \mathbf{v}_\tau^\top \left(\mathbb{I}_m^{\otimes 2} + \sin^2 \left(\theta_s^{(t)} + \frac{\pi}{4} \right) F \right) \mathbf{w}_\tau \\ &\quad - \sum_{\tau=t}^{T-1} \mathbf{v}_\tau^\top \left(\mathbb{I}_m^{\otimes 2} + \sin^2 \left(\theta_s^{(t)} - \frac{\pi}{4} \right) F \right) \mathbf{w}_\tau, \end{aligned} \quad (45a)$$

with

$$F = \left(S_s^{(t)} \right)^{\otimes 2} - \mathbb{I}_m^{\otimes 2}, \quad (45b)$$

where $\mathbf{v}_\tau, \mathbf{w}_\tau$ are some fixed vectors and $S_s^{(t)}$ is the swap corresponding to the parameter $\theta_s^{(t)}$. We note that the vectors $\mathbf{v}_\tau, \mathbf{w}_\tau$ may depend on the elements of $\boldsymbol{\theta}$ excluding the selected $\theta_s^{(t)}$. Equating (45a) with zero we obtain

$$\sin^2 \left(\theta_s^{(t)} + \frac{\pi}{4} \right) \sum_{\tau} (\mathbf{v}_\tau^\top F \mathbf{w}_\tau) = \sin^2 \left(\theta_s^{(t)} - \frac{\pi}{4} \right) \sum_{\tau} (\mathbf{v}_\tau^\top F \mathbf{w}_\tau), \quad (46)$$

then by (41d), we immediately see that the latter holds when $\sin \left(2\theta_s^{(t)} \right) = 0$, that is $\theta_s^{(t)} \in \Omega$. Consequently, points 1. and 2. follow.

For point 3., it is sufficient to show that $\mathbf{v}_\tau^\top F \mathbf{w}_\tau$ can be zero, then the value of $\theta_s^{(t)}$ is uninfluential. Therefore, the partial derivative w.r.t. the same variable is zero, independently from the value of $\theta_s^{(t)}$.

Vectors $\mathbf{v}_\tau, \mathbf{w}_\tau$ are the result of some DSM applied to the non-zero vectors, with non-negative entries, $\text{vec}_r(G^{(t)})$ and $\text{vec}_r(M_c)$. By Lemma A.3 the DSM action on those vectors preserves the ℓ_1 -norm, then $\mathbf{v}_\tau \neq \mathbf{0}, \mathbf{w}_\tau \neq \mathbf{0}$. Thus $\mathbf{v}_\tau^\top F \mathbf{w}_\tau = 0$ only as a result of the action of F . We show that there exist basis vectors $|a\rangle_m, |b\rangle_m$ such that the latter equality holds. Assume $S_s^{(t)} = \text{SWAP}_m(i, j)$ for some $i \neq j$ such that i, j are distinct from a, b , then

$$\langle a |_m^{\otimes 2} F | b \rangle_m^{\otimes 2} = \langle a |_m^{\otimes 2} \text{SWAP}_m(i, j)^{\otimes 2} | b \rangle_m^{\otimes 2} - \langle a |_m^{\otimes 2} | b \rangle_m^{\otimes 2} = 0, \quad (47a)$$

since $\text{SWAP}_m(i, j)$ fixes $|a\rangle_m, |b\rangle_m$. Hence there exist $\mathbf{v}_\tau, \mathbf{w}_\tau$ such that $\mathbf{v}_\tau^\top F \mathbf{w}_\tau$ vanishes, so point 3. is proved. \square

Lemma A.4. Consider the C^1 function $g: \mathbb{R}^n \rightarrow \mathbb{R}_+$, such that $g(\mathbf{x}^*) = 0 \implies \mathbf{x}^* \in \mathbb{Z}^n$ and $g(\mathbf{x} + 2\mathbf{e}_i) = g(\mathbf{x})$ for all $i = 0 \dots n-1$, with $\{\mathbf{e}_i\}$ the canonical basis for \mathbb{R}^n . In other words the zeros of g occur at points having integer entries, additionally the function is entry-wise periodic with fundamental period 2. Then the following optimization problems are equivalent

$$\begin{cases} \min_{\mathbf{w} \in \mathbb{R}^n} & \|\mathbf{w}\|_2^2, \\ \text{s.t.} & g(\mathbf{w}) = 0, \end{cases} \cong \begin{cases} \min_{\mathbf{w} \in \mathbb{R}^n} & \mathbf{card}(\mathbf{w}), \\ \text{s.t.} & g(\mathbf{w}) = 0, \end{cases} \quad (48)$$

where $\mathbf{card}(\cdot)$ denotes the cardinality of the argument.

Proof. A consequence of the periodicity is that for any $\mathbf{x} \in \mathbb{R}^n$ and $\mathbf{y} = (2 \sum_i k_i \mathbf{e}_i) \in 2\mathbb{Z}^n$, with $k_i \in \mathbb{Z}$, we have $g(\mathbf{x} + \mathbf{y}) = g(\mathbf{x})$.

Let $\mathbf{x}^* \in \mathbb{Z}^n$ fixed, and consider the *projection*¹⁷ $\mathfrak{P}_{2\mathbb{Z}}$ of \mathbf{x}^* onto the set $2\mathbb{Z}$, so let

$$\mathbf{y}^* \in \mathfrak{P}_{2\mathbb{Z}}(\mathbf{x}^*) = \operatorname{argmin}_{\mathbf{y} \in 2\mathbb{Z}^n} \{\|\mathbf{x}^* - \mathbf{y}\|_2^2\}, \quad (49)$$

then $\mathbf{x}^* - \mathbf{y}^* \in \{-1, 0, 1\}^n$, so

$$\|\mathbf{x}^* - \mathbf{y}^*\|_2^2 = \sum_i (x_i^* - y_i^*)^2 = \sum_i |x_i^* - y_i^*| \quad (50a)$$

$$= \|\mathbf{x}^* - \mathbf{y}^*\|_1 \quad (50b)$$

$$= \mathbf{card}(\mathbf{x}^* - \mathbf{y}^*) \quad (50c)$$

Now, consider the first optimization problem in (48) and perform the substitution $\mathbf{w} = \mathbf{x} - \mathbf{y}$, to obtain

$$\begin{aligned} \min_{\mathbf{x} \in \mathbb{R}^n, \mathbf{y} \in 2\mathbb{Z}^n} \|\mathbf{x} - \mathbf{y}\|_2^2, \\ \text{s.t. } g(\mathbf{x} - \mathbf{y}) = g(\mathbf{x}) = 0. \end{aligned} \quad (51)$$

Let $G = \{\mathbf{x} \in \mathbb{R}^n | g(\mathbf{x}) = 0\}$ be the set of feasible points, then by assumption, $\mathbf{x} \in G \implies \mathbf{x} \in \mathbb{Z}^n$, that is $G \subset \mathbb{Z}^n$. Since the constraint is independent from the variable \mathbf{y} , we rewrite the optimization problem considering the feasible set, so

$$\min_{\mathbf{x} \in G, \mathbf{y} \in 2\mathbb{Z}^n} \|\mathbf{x} - \mathbf{y}\|_2^2, \cong \min_{\mathbf{y} \in 2\mathbb{Z}^n} \min_{\mathbf{x} \in G} \|\mathbf{x} - \mathbf{y}\|_2^2, \quad (52)$$

then by (49) and (50a), the optimal \mathbf{y}^* is the one such that $\mathbf{x}^* - \mathbf{y}^* \in \{-1, 0, 1\}^n$ and the cardinality of $\mathbf{x}^* - \mathbf{y}^*$ is minimized. Hence the equivalence in (48) is established. \square

Proof of Proposition 3.2. We sketch a proof based on Lemma A.4. The aforementioned lemma can be adapted to the periodicity of the hardware cost function \mathcal{L} . It follows from (16b) that the period of \mathcal{L} is π . Define the function

$$g(\mathbf{x}) = \mathcal{L}\left(\frac{\pi\mathbf{x}}{2}\right), \quad (53)$$

which has period 2. Also the cardinality function is invariant to a non-zero vector scaling, that is $\mathbf{card}(\mathbf{x}) = \mathbf{card}(\alpha\mathbf{x})$ for all $\alpha \in \mathbb{R} \setminus \{0\}$. Then by applying Lemma A.4, the claim follows. \square

Proof of Lemma 3.5. Under the assumptions that $P_a^2 = P_b^2 = \mathbb{I}_m$ and $P_a P_b = P_b P_a$ we obtain that $(P_a P_b)^2 = P_a P_b P_a P_b = P_a P_b P_b P_a = \mathbb{I}_m$, then we need that

$$(P_a + P_b - \mathbb{I}_m)^2 = \mathbb{I}_m + 2[P_a P_b - (P_a + P_b - \mathbb{I}_m)] = \mathbb{I}_m, \quad (54)$$

which is true if and only if $P_a P_b = (P_a + P_b - \mathbb{I}_m)$. The latter being the claim proves the lemma. \square

Proof of Proposition 3.6. First we note that, for $m \times m$ permutation matrices P_a, P_b , fulfilling the conditions of Lemma 3.5, then

$$(P_a - \mathbb{I}_m)(P_b - \mathbb{I}_m) = P_a P_b - P_a - P_b + \mathbb{I}_m \stackrel{(27)}{=} 0. \quad (55)$$

¹⁷We highlight a technicality regarding the projection $\mathfrak{P}_{2\mathbb{Z}}$. Since the set $2\mathbb{Z}^n$ is non-empty closed but non-convex, then we cannot assure that the projection is a singleton [2, first projection theorem], consequently we assume $\mathfrak{P}_{2\mathbb{Z}}$ to be a set-valued operator, with the non-emptiness resulting from the set $2\mathbb{Z}^n$ being non-empty and close.

In other words, given any pair of distinct, commuting and involutory permutations (acting on the same vector space), the product of their shift by the identity vanishes.

We proceed by induction. Equation (29) is clearly true for $n = 1$, furthermore, assume it is true for an arbitrary $n \geq 1$, then consider the case $n + 1$ by multiplying both sides of equation (29) by $\mathbb{I}_m + \sin^2(\theta_{n+1})(P_{n+1} - \mathbb{I}_m)$ to get

$$\prod_{t=1}^{n+1} (\mathbb{I}_m + \sin^2(\theta_t)(P_t - \mathbb{I}_m)) = \mathbb{I}_m + \sum_{t=1}^{n+1} \sin^2(\theta_t)(P_t - \mathbb{I}_m) \quad (56a)$$

$$+ \sum_{t=1}^n \sin^2(\theta_t) \sin^2(\theta_{n+1}) \underbrace{(P_t - \mathbb{I}_m)(P_{n+1} - \mathbb{I}_m)}_{0 \text{ by (55)}} \quad (56b)$$

$$= \mathbb{I}_m + \sum_{t=1}^{n+1} \sin^2(\theta_t)(P_t - \mathbb{I}_m), \quad (56c)$$

hence the claim is proved. □